CLF Annual Report : Proton probing of the reconnecting magnetic fields surrounding two adjacent, high-intensity laser interactions

Contact: charlotte.palmer@cockcroft.ac.uk

C. A. J. Palmer, Y. Ma and M. J. V. Streeter.
The Cockcroft Institute/Lancaster University

P. T. Campbell, P. Kordell, K. Krushelnick, A. G. R. Thomas and and L. Willingale.
University of Michigan

L. Antonelli, C. R. Ridgers and N. Woolsey.
University of York

J. Halliday, E. R. Tubman and S. Lebedev.
Imperial College London

Y. Katzir, E. Montgomery and M. Notley.
Central Laser Facility

Abstract

Magnetic reconnection is a process that contributes significantly to plasma dynamics and energy transfer in a wide range of situations, including inertial confinement fusion experiments, stellar coronae and compact, highly magnetised objects like neutron stars. There are many different models to describe this phenomena and laboratory experiments are used to refine these models and assess their applicability. Magnetic fields can be generated using high power lasers through several mechanisms, most famously the Biermann battery associated with the formation of azimuthal magnetic fields around a laser focus due to non-parallel gradients in electron temperature and density. At high laser intensities ($I_L\lambda_L^2 > 10^{18}$ Wcm$^{-2}\mu$m^2), relativistic surface currents play a significant role in the generation of the azimuthal magnetic fields. Experiments exploring magnetic reconnection at moderate intensities ($I_L \sim 10^{14}$ Wcm^{-2}) have been performed at numerous international facilities. Here, we present on-going analysis of reconnection fields measured during a recent experiment that utilise laser intensities close to 10^{18} Wcm^{-2} to approach the relativistic regime.

1 Introduction

Magnetic reconnection is a fundamental process with relevance to plasma physics at both astrophysical and terrestrial scales [1][2][3]. The process itself involves a change in topology of magnetic field lines in which field lines are broken and reconnect in a lower energy geometry. During this restructuring, magnetic energy is released. The exact details of the process and the energy release are under investigation for different conditions, with several models explaining some, although not all, of the observations that have been associated with reconnection.

Intense laser pulses can be used to generate strong magnetic fields in the laboratory and these pulses have been exploited in recent years to study reconnection at intensities on the level of 10^{14} Wcm^{-2} [4, 5]. Through the exploitation of chirped pulse amplification, relativistic intensity laser fields can be produced. This affects magnetic field generation and has been demonstrated to produce field strengths with $\mathcal{O}(100)$ MG magnitude, that are transported by electron flows with velocities close to the speed of light [6].

When two such laser pulses are focused to within several spot diameters of each other, these rapid plasma flows bring together anti-parallel magnetic fields that are presumed to reconnect, with reconnection following a collisionless relativistic model [7]. This provides the opportunity to study relativistic reconnection, relevant to astrophysical plasmas associated with highly magnetized, compact objects such as neutron stars and black holes in the laboratory and develop the model of reconnection in this regime.

Experiments at the HERCULES and OMEGA EP facilities have performed experiments in this regime studying the x-ray emission associated with two high intensity laser spots with variable spot separation [8]. The measurements show strong localised k-alpha emission from the midplane between the two laser spots generated by the interaction of 'hot' electrons with the cold target. It is determined that the radiation is emitted from depths > 10 μm within the target, illustrative of the generation of a hot electron population with energy 100 keV generating the signal. This signal was only present when the two laser spots are simultaneously incident at the target surface. In the case of reconnection between the magnetic fields surrounding the two laser spot, an electric field is established in the reconnection region. This field is oriented perpendicular to the surface such that electrons would be accelerated into the target. Additional measurement of the electron spectra from the target indicate a non-thermal electron population, again present only when both spots are simultaneously incident on the target. While these measurements provide a strong indication of reconnection at the midplane, observation of dynamically changing magnetic fields surrounding the focal spots would be extremely valuable.

Target Area West of the VULCAN laser facility offers two high intensity laser pulses with flexible geometry. The inclusion of a split mirror in one beam allows the production of two focal spots, whose separation can be varied by adjustment of the mirror, with one of these beams, while the other can be tightly focused and used to generate a proton beam via TNSA [9]. Proton beams produced by this technique are non-relativistic and exhibit low emittance and broad energy spread, which makes them ideally suited to probe the dynamically changing electric and magnetic fields associated with dense plasma interactions [10]. The non-relativistic beam spreads in time, allowing the same beam to probe the plasma interaction at multiple times. Subsequent energy resolved measurement of the spatial profile of these beams can identify the deflection due to the plasma fields and use this to estimate the field strength. While both strong electric and magnetic fields are associated with the interaction of high intensity laser pulses with the plasma target, the electric field has been demonstrated to be primarily directed normal to the target surface [11]. Therefore if probing proton beam is set up to be directed along this axis, the deflection can be assumed to be due in the most part to the magnetic fields.

The experiment described here was designed to use the flexible TAW dual beam geometry with the split mirror, to probe the dynamic evolution of fields associated with the interaction of two high intensity laser focal spots. The inclusion of electron spectrometers at multiple angles and a k-alpha diagnostic were planned to verify the comparison of these field measurements with the data previously taken during the HERCULES and OMEGA EP experiments. In addition, the flexible setup permitted electron spectrometer measurements over a wider range of angles, and it was hoped that this would show whether the non-thermal component of the hot electron spectrum was confined within a solid-angle or present throughout the highly divergent electron beam.

The setup of the laser and the proton probing diagnostic will be outlined below. Images from the proton probing will be presented illustrating qualitative differences between the fields formed with targets of different materials and with varying separation of the two high intensity laser spots. We will also outline our plans for the continued analysis. For comparison, proton probing of the magnetic fields surrounding a single high-intensity laser pulse at the same laser facility is presented in [11].

2 Experimental setup

The experiment was performed using the two CPA laser pulses of the Target Area West laser facility. The beams, referred to as the main beam and the probe beam, had pulse durations of 9.6 ps and 1.6 ps respectively, both with a central wavelength of ~ 1 μm and linear polarisation.

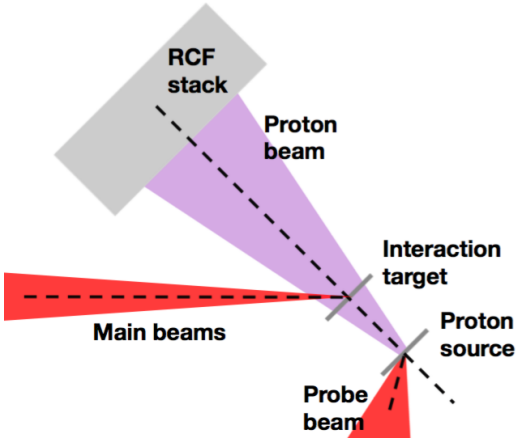

Figure 1: Schematic of the experimental arrangement of the proton probing diagnostic. The incidence angle of the main beams was set to 45°, with a separation of 3 mm between the proton source and the interaction target. A copper mesh was placed between these two foils at 1.5 mm from each. The distance from the interaction to the RCF detector stack was set to 40 mm.

In the path of the main laser beam, a split mirror positioned before the focusing optic was used to produce two focal spot whose relative position could be adjusted by adjusting the split mirror. The focusing optic was a f/15 off-axis parabolic mirror that produced a FWHM of each focal spot of 30 μm, assuming a compressor throughput of 60% and averaging the measured laser beam energy energy over the studied shots (220±27 J), this corresponds to an on-target intensity of $7{\times}10^{17}$ Wcm^{-2}. The main target consisted of one of four options: a) 30 μm thick polypropylene (PP) film, b) 10 or 25 μm thick Cu foil, c) 15 μm thick Al foil. The surface normal of these planar targets was orientated at 45° to the incoming laser axis.

The second (probe) laser beam, was used for production of the proton probe through TNSA of a non-relativistic, broadband proton beam from a thin (15 μm) Al target foil. The probe laser beam was focused using an f/3 off-axis-parabolic mirror to a FWHM spot size of 3.6 μm, corresponding to an average peak intensity of $2{\times}10^{20}$ Wcm^{-2}, assuming again 60% energy throughput of the compressor and averaging the energy of the shots (89 ± 19 J). The incidence angle of the laser beam with respect to the target surface normal was approximately 60°. This was as a result of geometric constraints on the input beam and off-axis angle of the parabolic mirror, and lead to an elongation of the focal spot at the target surface to form an ellipse with long axis 7.2 μm. This increase in area of the focus lead to a reduction in peak intensity of $I_0/2 = 1 \times 10^{20}$ Wcm^{-2}. The relative timing of the probe beam and the main interaction beam could be varied using a delay stage before the compressor.

The proton beams produced by this interaction were found to be lower in energy than expected, regularly reaching a maximum energy of 8 MeV potentially due to ASE. The arrangement of the proton target relative to the main interaction target was such that the proton beam axis could be aligned either with the surface normal of the main interaction target, passing from the rear to the front surface of the main target (rear probing geometry), or, through rotation of the main interaction target by 90° about the vertical axis, parallel with the main interaction target surface (side probing geometry). Figure 1 illustrates the setup for the rear probing geometry for which we expect magnetic fields formed at the front surface to deflect the protons out from the central region [11]. The distance between the main interaction target and the proton source was set to 3 mm. On the majority of the shots, a Cu mesh, with thickness of 25 μm and wire spacing of 63 μm, was positioned between the proton source and the main interaction target at 1.5 mm from both foils. This mesh will be used to determine the deflection of the protons in the interaction fields, relative to their initial trajectory.

The energy resolved detector for the proton beam utilised stacks of radiochromic films (HD-V2 and EBT-XD), and was protected from the laser light with an aluminium housing. The proton beam had to penetrate Aluminium foil with thickness of 20 μm to reach the films. The stack was positioned at 40 mm from the main interaction target, leading to a magnification of the interaction onto the stack of ≈14. In the following section the data is presented with the spatial axes taken as the dimensions at the interaction plane.

The auxiliary diagnostics included six electron spectrometers. These small spectrometers utilised magnetic dipoles behind 500 μm slit to disperse the electron beam onto an image plate. The energy range covered by the image plate corresponded to 1 - 40 MeV. The spectrometers were positioned approximately 20 cm from the main interaction target, with five of them in the horizontal plane at angles corresponding to -30°, 0°, 30°, 60° and 90°, around the surface normal of the main target. The sixth spectrometer was also positioned at 90° to the main interaction target surface normal, but in the vertical plane. The data from the electron spectrometers indicates deflecting fields transverse to the designed fields of the dipole, that result in caustic features at the image plate. A full 3-D field map for the spectrometer magnets is required to retrieve the electron energy spectra.

3 Results

The rear probing data set contains interactions with different main target material, and with different focal spot separation (435 μm, 820 μm). Figure 2 presents raw RCF films corresponding to 3.5 MeV proton beams which have probed the main interaction at a time corresponding to 54 ps after fields are first observed in the probing images. The different images correspond to main interaction targets of different material (Cu, Al, PP) with target Z deceasing from left to right.

With the metal targets, we saw a lot of scattering in the probing proton beam, such that the modulation induced by the mesh was not visible for any probing proton energy. Despite the scattering, cavitation of the proton signal is still visible, producing two 'bubbles' with enhanced proton signal around their circumference. The size of the proton bubbles appear smaller for the metal targets than for the plastic target for the same probing time and proton energy. This reduced proton deflection implies either smaller absolute field strengths, smaller extension of the magnetic field transversely along the target surface, or longitudinally in the target surface plasma.

In the absence of an observable mesh, the magnetic field maps will be approximated by employing analysis that studies the variation in local proton flux, assuming an initially smooth proton distribution [12]. Although this technique has been developed for use without a mesh, it may also prove valuable for this data.

From the selection of plastic targets there are also two different focal spot separations available (435 μm and 820 μm). Examples of these are shown in figure 3. Qualitatively, these show significantly more disruption to the mesh structure within the magnetic field 'bubbles' for the smaller (435 μm) separation than the larger, with enhanced proton flux pile-up at the edge of the ring. While the larger (820 μm) separation, exhibits a circular shape, the magnetic field deflection for the 435 μm separation appears more elliptical with the long axis of the ellipse parallel with the midplane of the reconnection. The predominantly circular shape of the large separation interaction highlights the deformity of the region between the two laser foci. Here the circular shape of each 'bubble' is flattened as they interact with one another, with a pile up of proton flux in the midplane region. The mesh structure is visible both outside and, to a certain extent, within the bubbles, and it is clear to see that the proton trajectories have not crossed the midplane. Assuming proton deflection would be radially symmetric in the absence of the second laser spot, matching with published measurements [11], this implies that the protons deflected by one focus encounter a restoring force that adjusts their path towards the target normal.

4 Conclusion

Magnetic reconnection with high intensity laser pulses is currently being explored by a series of experiments at several laser systems. The work using the VULCAN TAW laser facility was aimed at measuring the temporal evolution of the magnetic fields around two laser pulses, and to probe the changes in these fields due to their interaction with one another, using a broadband, proton beam.

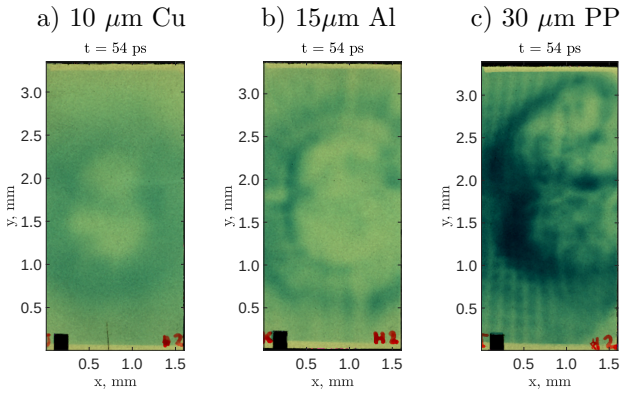

Figure 2: 3.5 MeV proton flux distributions in the form of scanned radiochromic film for different target materials a) 10 μm Cu b) 15 μm Al c) 30 μm PP (Plastic). The point in time at which the proton probe crosses the main interaction is given above the images. In all cases the focal spot separation was set to 435 μm and a Cu mesh was included in the proton probing beam before the interaction. This is only visible in c) due to increased scattering in the metal targets.

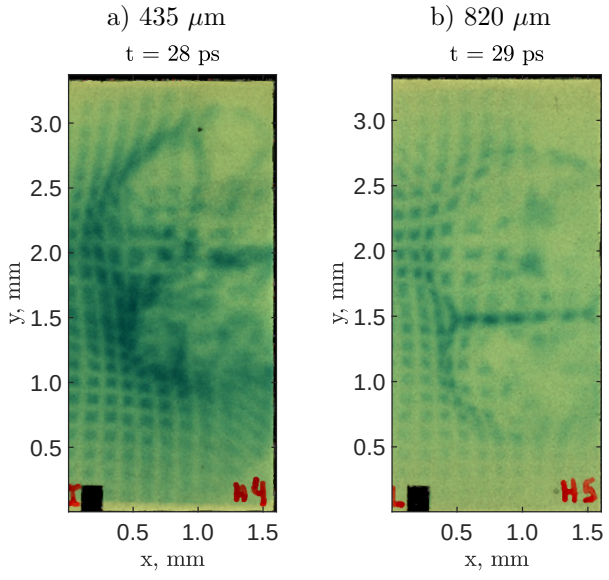

Figure 3: Proton flux distributions for different laser focal spot separations of a) 435 μm b) 820 μm with plastic targets.

Preliminary data reveals qualitative differences between the magnetic field structure depending on the material of the main interaction target, and the separation of the laser focal spots at the target surface. Analysis is underway to map the distortion of the grid-like modulation imposed on the beam, which can be used to infer the magnetic field strengths at different points of the interaction.

Acknowledgements

The authors would like to acknowledge the support of the Central Laser Facility VULCAN engineering, laser and target area support teams without whom this work would not be possible. We also acknowledge financial support from the STFC Cockcroft Institute Core Grant ST/G008248/1 for supplying the consumable diagnostics, and the Department of Energy National Nuclear Security Administration, under Award Number DE-NA0002727, for supporting our US participants.

References

[1] M. Hoshino and Y. Lyubarsky. Relativistic Reconnection and Particle Acceleration. *Space Science Reviews* **173,** 1-4 (2012), pp. 521–533.

[2] J. A. Goetz, R. N. Dexter, and S. C. Prager. Total-magnetic reconnection during a major disruption in a tokamak. *Physical Review Letters* **66,** 5 (1991), pp. 608–611.

[3] J. D. Hare et al. Anomalous Heating and Plasmoid Formation in a Driven Magnetic Reconnection Experiment. *Physical Review Letters* **118,** 8 (2017), p. 085001.

[4] P. M. Nilson et al. Magnetic Reconnection and Plasma Dynamics in Two-Beam Laser-Solid Interactions. *Physical Review Letters* **97,** 25 (2006), p. 255001.

[5] C. K. Li et al. Observation of megagauss-field topology changes due to magnetic reconnection in laser-produced plasmas. *Physical Review Letters* **99,** 5 (2007), pp. 1–4.

[6] W. Schumaker et al. Ultrafast Electron Radiography of Magnetic Fields in High-Intensity Laser-Solid Interactions. *Physical Review Letters* **110,** 1 (2013), p. 015003.

[7] Ellen G. Zweibel and Masaaki Yamada. Magnetic Reconnection in Astrophysical and Laboratory Plasmas. *Annual Review of Astronomy and Astrophysics* **47,** 1 (2009), pp. 291–332.

[8] A. Raymond et al. Relativistic Magnetic Reconnection in the Laboratory (2016). arXiv: 1610.06866.

[9] Stephen P. Hatchett et al. Electron, photon, and ion beams from the relativistic interaction of Petawatt laser pulses with solid targets. *Physics of Plasmas* **7,** 5 (2000), p. 2076.

[10] M. Borghesi et al. Laser-produced protons and their application as a particle probe. *Laser and Particle Beams* **20,** 02 (2002), pp. 269–275.

[11] G. Sarri et al. Dynamics of Self-Generated, Large Amplitude Magnetic Fields Following High-Intensity Laser Matter Interaction. *Physical Review Letters* **109,** 20 (2012), p. 205002.

[12] A. F. A. Bott et al. Proton imaging of stochastic magnetic fields. *Journal of Plasma Physics* **83,** 06 (2017), p. 905830614.